Optimization of Non-uniform Planar Coils in Wireless Power Transfer Systems Using Resonant Converters

Ghovindo Siadari

A thesis
submitted in partial fulfillment of the
requirements for the degree of

Master of Science

University of Washington

2024

Committee:

Jungwon Choi

Daniel Kirschen

Program Authorized to Offer Degree:

Electrical and Computer Engineering

University of Washington

Abstract

Optimization of Non-uniform Planar Coils in Wireless Power Transfer Systems Using Resonant Converters

Ghovindo Siadari

Chair of the Supervisory Committee:

Jungwon Choi

Electrical and Computer Engineering

The new era of mobility has pushed a rapid adoption of electric vehicles (EVs). Since then, many efforts have been made to make the experience of driving EVs more comfortable, including how to charge them. Wireless power transfer (WPT), also known as wireless charger, has caught much attention from researchers and industries since it is seen as a more practical and convenient way of charging EVs.

This thesis will discuss a systematic approach to designing a WPT system, from the selection of the converter to the tuning process and coil design. It will also introduce a new approach to modeling the WPT coil. Using the new modeling, a mathematical optimization will be conducted to maximize the quality factor of the coils, which will increase the efficiency of the WPT systems.

By Implementing the methodology explained above, a class Φ_2 with optimized transmitter coils and receiving coils is selected for the WPT systems. A 230 V voltage level and 13.56 MHz frequency are selected as the operating conditions of the WPT systems. The WPT systems are fabricated and tested in burst mode. The experimental result confirms that the WPT system can deliver 1072 W output power with 96% efficiency over 63 mm distance, which proves the effectiveness of this WPT system.

Contents

List of Figures

List of Tables

Chapter 1 Introduction

1.1 Background

The 21st century has seen significant technological advancements, particularly in machinery, digital technology, and electrical devices. However, the rapid adoption of these technologies has consequences. Every mile traveled, watt of electricity consumed, and byte of data processed contributes to a carbon footprint [1,2]. Whether it's the emissions from cars, and power plants, or the environmental impact of resource extraction for gadgets, these activities harm the planet. In response, efforts have been made to mitigate these effects. These include developing renewable energy sources, improving combustion technology, and promoting electric vehicles (EVs) as an eco-friendly transportation option.

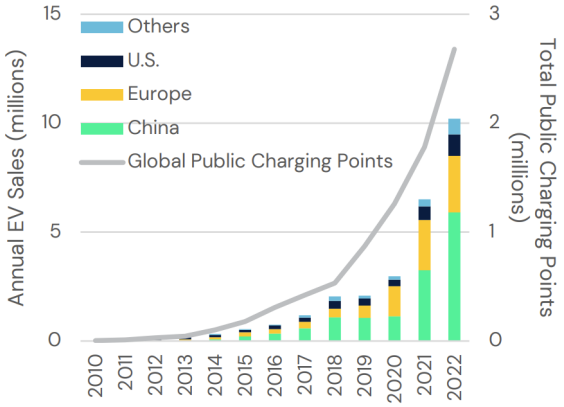

Figure 1: Worldwide EV Growth Projection. [12]

The need to reduce carbon emissions has led to the rise of electric vehicles (EVs) as a new mode of mobility. While EVs offer environmental benefits, they also come with drawbacks. One major issue is related to battery charging. In addition to long charging times, convenience is a concern, with users having to handle bulky and heavy charging cables. Wireless power transfer (WPT) with high power capabilities is being explored as a potential solution, eliminating the need for a physical connection between the charger and the EV.

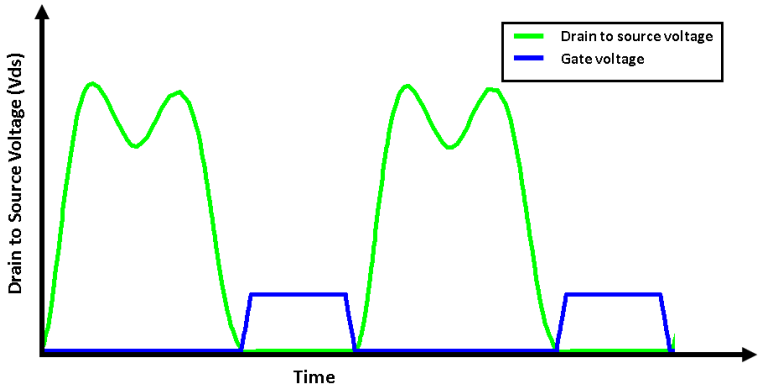

Figure 2: Zero Voltage Switching.

The resonant converter is favored in high-frequency applications compared to other traditional converters due to its ability to operate at high frequencies, which is beneficial for miniaturizing the size of the converter and WPT coil. Additionally, the resonant converter can operate in zero voltage switching (ZVS) mode that ensures the switch turns on when the voltage across it is zero or very close to zero, as can be seen in Figure 2. This thing will ensure that there are minimal losses on the switch when it is on thus improving the efficiency of the converter, especially at high frequency.

One of the most popular coils in WPT is the circular coil. This coil has a simple shape and is well-optimized. Traditional WPT coils utilize an external capacitor as a series compensator to optimize power transfer between the transmitter (Tx) and receiver (Rx) coils. However, this method has a disadvantage: the external capacitor suffers from high voltage stress. Another method often used is the open-type coil, which utilizes the parasitic capacitor between the two coils on both the Tx and Rx sides.

As the title suggests, this thesis will focus on electric vehicle technology, specifically the power electronic and wireless power transfer side. This chapter will explore more about the state of the art of power electronics for EVs relevant to this thesis.

1.2 Resonant Converter Technology

Power converters play a huge role in the growth and adoption of EVs. They convert electrical power from one form to another. Various research and development efforts have been made to make converters more efficient, smaller in size, and with higher power density. A higher power density in a converter can be achieved by increasing the operating frequency, as this allows for the use of smaller passive components such as capacitors and inductors. Even though this method is useful for reducing the size of the converter, careful consideration must be taken when increasing the operating frequency, especially with conventional pulse width modulation (PWM) converters such as buck, boost, or buck-boost converters. These traditional converters use hard switching to convert electric power, meaning the switch turns on when the voltage across it is not zero. This method causes power losses in the switch (P_{sw}), which become higher as the frequency increases:

$$P_{sw} \propto f_{sw}. \tag{1}$$

A very high operating frequency is beneficial in reducing the size of a converter, thus achieving a higher power density. Unfortunately, the operating frequency of conventional converters is limited by losses caused by hard switching. Another type of converter that can operate at high frequencies is the resonant converter. It operates based on the principle of resonance, where energy is stored and transferred between the converter components at the resonant frequency. This type of converter is favored over PWM converters due to its ability to operate at ultra-high frequencies while maintaining minimal switching losses at those frequencies (MHz). These minimal switching losses are achieved through careful tuning, enabling the converter switch to turn on and off when the voltage across it is zero or in ZVS mode.

There are several resonant converters that can achieve zero voltage switching operation, such as full bridge and dual active bridge converter (DAB). Those two converters can operate at high frequency in ZVS mode, thus minimizing the losses. Unfortunately, several switches are required, which, in consequence, will make the

control of the converter more complex and could reduce its reliability [13]. To address that issue a derivation of radio frequency (RF) amplifiers is proposed such as class E, class DE, and class Φ_2 converter. Those inverter uses a significantly lower number of switches to increase the reliability of the converter.

For example, the Class E converter, shown in Figure 3, is also widely used as a resonant converter [10]. This converter only uses one switch, which improves its reliability and efficiency. However, this converter suffers from high voltage stress across the switch, reaching four times the input voltage. As a result, this converter is limited to operating at low voltage to avoid damaging the switch, making it only suitable for low-power applications. The Class DE converter, as depicted in

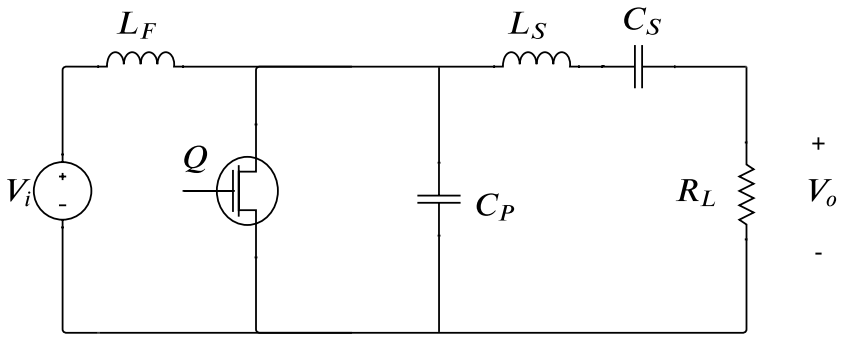

Figure 3: Class E Inverter.

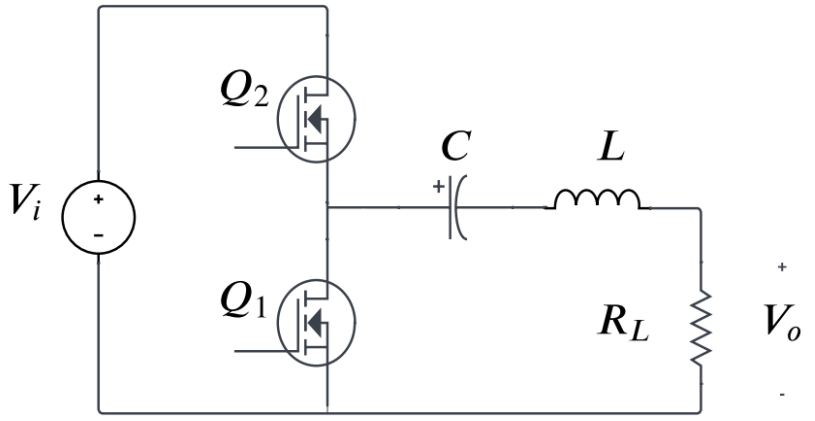

Figure 4: Class DE Inverter.

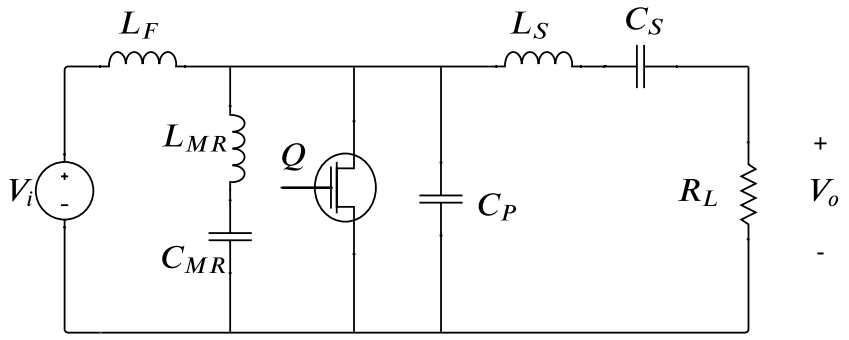

Figure 5: Class Φ_2 Inverter.

Table 1: Resonant Converter Types

Converter	V_{ds}	**Number of Switches**	**Number of passive components**
Class E	$4 \times V_{in}$	1	4
Class DE	$1 \times V_{in}$	2	4
Class Φ_2	$2 \times V_{in}$	1	6

Figure 4, has lower voltage stress across the switch [15]. However, it requires two switches, which can affect reliability and efficiency. To address the issue of high voltage stress and reliability, a class Φ_2, shown in Figure 5, converter is introduced. This converter only requires one switch, which is desirable for easier control, more efficient, and more reliable operation. Moreover, the voltage across the switch of this converter is only two times the input voltage that enables it to operate at a higher voltage level. This converter requires more passive components, but later, we can see that the size of passive components for this converter is relatively small compared to other resonant converters. Table 1 summarizes the types of resonant converters. From the explanation above, it is clear that the class Phi_2 converter is superior compared to another converter since it is more reliable and can operate at higher voltage levels, thus making it a potential inverter for the WPT system. Due to that reason, this paper will explore more about the class Φ_2 converter.

The Class Φ_2 converter was first introduced by Rivas et al. in 2008. The Class Φ_2 converter has an almost similar topology to the Class E converter, as shown in Figures (5) and (3). The difference lies in the additional branch circuit that

is parallel to the switch. This parallel branch contains an inductor (L_{MR}) and capacitor (C_{MR}), which are responsible for lowering the switch's peak voltage, thus allowing the converter to operate at higher voltage [4, 6], resulting in an increased power level.

The first step to designing the class Φ_2 converter is to choose the value of L_s, which can be calculated using the formula in equation (2) after determining the input voltage V_i, switching frequency f_{sw}, output power P_{out}, and load resistance R_L. The value of C_S can be chosen arbitrarily as long as it is large enough to block the DC voltage. Therefore, L_s is calculated, as shown below:

$$L_s = \frac{1}{\omega_{sw}} \sqrt{R_L * (\frac{8V_i^2}{\pi^2 P_{out}}) - R_L}. \tag{2}$$

The next step is to calculate the impedance of Z_{MR}, which is the series impedance of L_{MR} and C_{MR}. As shown in equation (3), the value of L_{MR} and C_{MR} must be tuned such that the impedance of Z_{MR} resonates at the second harmonic (ω_{2sw}):

$$Z_{MR}(\omega_{2sw}) = j2\omega_{2sw}L_{MR} + \frac{1}{j2\omega_{2sw}C_{MR}} = 0. \tag{3}$$

Then, the drain-to-source impedance can be calculated by taking the parallel impedance of the Z_L and Z_{MR}:

$$Z_{\mathrm{DS}}(w) = Z_{\mathrm{MRP}} // Z_L, \tag{4}$$

where Z_{MRP} is the parallel impedance of the L_{MR} and C_{MR}, L_f, and C_{OSS} and C_P. Z_L can be calculated by taking the series impedance of the L_S, C_S, and R_L as shown below:

$$Z_{\mathrm{MRP}}(w) = wL_f // \left(jwL_{\mathrm{MR}} + \frac{1}{jwC_{\mathrm{MR.}}} \right) // \frac{1}{jw(C_{\mathrm{OSS}} + C_P)} \tag{5}$$

$$Z_L(w) = jwL_S + \frac{1}{jwC_S} + R_L. \tag{6}$$

To achieve ZVS switching operation, first, the drain to source impedance of the converter must be inductive at switching frequency:

$$30^\circ < \angle Z_{DS}(\omega_{sw}) < 60^\circ. \tag{7}$$

And, the magnitude of the drain to source impedance at switching frequency (ω_{sw}) must be at least 8 dB lower than the magnitude at the third harmonic (ω_{3sw}) :

$$|Z_{DS}(w_{sw})| - |Z_{DS}(3w_{sw})| < 8dB. \tag{8}$$

Lastly, the drain-to-source impedance at the third harmonic must be capacitive with a phase angle lower than -80°, as shown below:

$$\angle Z_{DS}(3w_{sw}) < -80^\circ. \tag{9}$$

To summarize, the tuning process should follow the equations (2) to (5). This tuning process will ensure the converter operates at ZVS mode. Figure 6 shows how the drain to source impedance's magnitude and phase should look when the tuning of the class Φ_2 converter is correct. The plot shows the drain to source impedance magnitude and phase of a class Φ_2 converter with an operating frequency of 13.56 MHz.

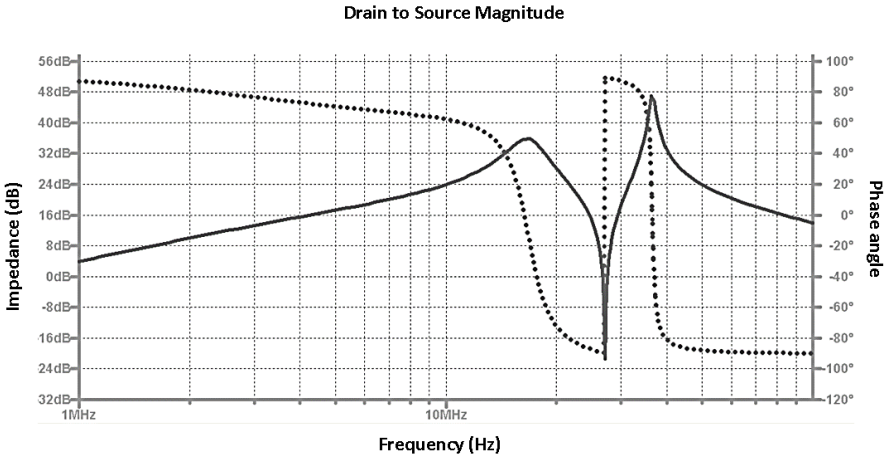

Figure 6: Magnitude and Phase of class Φ_2 Inverter.

1.3 Wireless Power Transfer (WPT) Coil

Inductive power transfer (IPT) is a well-known method to transfer electrical power wirelessly with high efficiency for a mid-range application. This system transfers power from a TX coil to an Rx coil through a magnetic field. IPT works efficiently at high frequency, in addition, frequency operation can reduce the overall size of the WPT system [16]. However, designing the IPT at high frequency poses its challenges. High-frequency current tends to flow at the coil's surface known as the skin effect. This skin effect will cause higher series resistance compared to when the IPT works at a lower frequency. This higher series resistance will cause more losses in the coil and reduce the quality factor which eventually significantly lowers the overall WPT system efficiency.

IPT works based on Ampere's and Faraday's laws. Ampere's law states that the magnetic field B around a closed loop is proportional to the electric current I passing through the loop. Mathematically, Ampere's Law is often written in integral form as equation (10), where $\oint \mathbf{B} \cdot d\mathbf{l}$ is the line integral of the magnetic field $\mathbf{B}$ around a closed loop, μ_0 is the permeability of free space, and $I_{enclosed}$ is the total current passing through any surface bounded by the closed loop:

$$\oint \mathbf{B} \cdot d\mathbf{l} = \mu_0 I_{\text{enclosed}}. \tag{10}$$

Faraday's law describes how a changing magnetic field can induce an electromotive force (EMF) in a nearby conductor. The mathematical representation of this law can be written as equation (11) where e is the induced electromotive force (EMF) in volts (V) and $\frac{d\Phi}{dt}$ is the rate of change of magnetic flux (Φ) through the loop with respect to time (t):

$$e \propto -\frac{d\Phi}{dt}. \tag{11}$$

Using the above principles, a WPT coil can be constructed where the TX coil operates based on Ampere's law with an AC voltage source to produce a time-varying magnetic field. The RX part of the WPT coil operates based on Faraday's law to generate an EMF from time-varying magnetic fields that come from the RX coil.

The TX and RX coils are separated by an air gap and linked by a magnetic field. The amount of magnetic field from the TX coil that the RX coil can capture is influenced by the coupling coefficient k. The larger the distance of the air gap, the smaller the value of k, which will affect the WPT efficiency. To efficiently transfer power over a large distance, a very high magnetic field is required. One prevalent method to achieve this is through a resonant WPT coil, which can be realized by using an external capacitor in series with the WPT coil, also known as magnetic resonant coupling. The capacitance of the capacitor is tuned such that resonance is achieved at the operating frequency:

A coil can transfer power more efficiently when operating at ultra-high frequency [8]. Moreover, the efficiency can be further increased when the coil works at resonant conditions. An external capacitor is usually placed in series with the coil to achieve resonance. However, operating under such conditions will subject the external capacitor to high voltage stress, making it prone to breakdown.

Open-type four-coil systems are often used to overcome this issue. A set of two

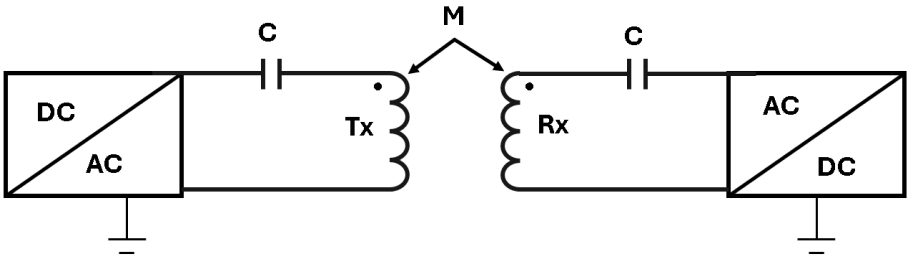

Figure 7: Magnetic Resonant Coupling.

coils for each RX and TX side can provide internal capacitance, as depicted in Figure 8. The capacitance of the coil can be adjusted by changing the distance between coils on the RX and TX sides. To improve the quality factor and efficiency of the coil, a planar open coil type made from a copper sheet is proposed. Manufacturing the coil from planar material instead of a round conductor can reduce the resistance that arises from the skin effect.

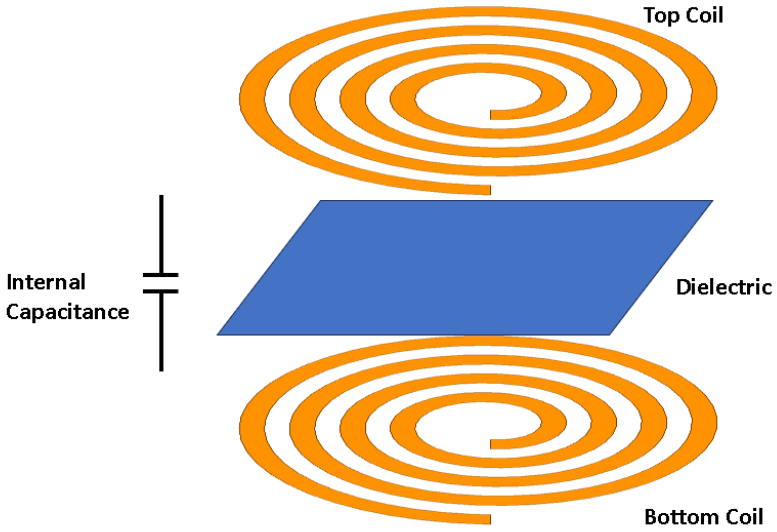

Figure 8: Open-type Coil.

The inductance of the coil can be improved by increasing the width of the coil or increasing the number of turns. However, this approach will increase the capacitance, which then decreases the resonant frequency, thus lowering the converter's efficiency and ultimately affecting the overall system size. A non-uniform system is

designed by [3] to address this issue. By making the coil's width non-uniform, the coil's capacitance can be adjusted to maintain a high resonant frequency.

The inductance and resistance calculation for a planar coil has been investigated by [7]. The inductance of a single planar coil (L_s) is given by equation (12) where μ is the magnetic permeability, d_o is the outer diameter of the coil, and d_i is the inner diameter of the coil:

$$L_s = \frac{\mu n^2 (d_i + d_o)}{4} \left(\ln \frac{2.46(d_i + d_o)}{d_o - di} + 0.2 \left(\frac{d_o - d_i}{d_o + d_i} \right)^2 \right). \tag{12}$$

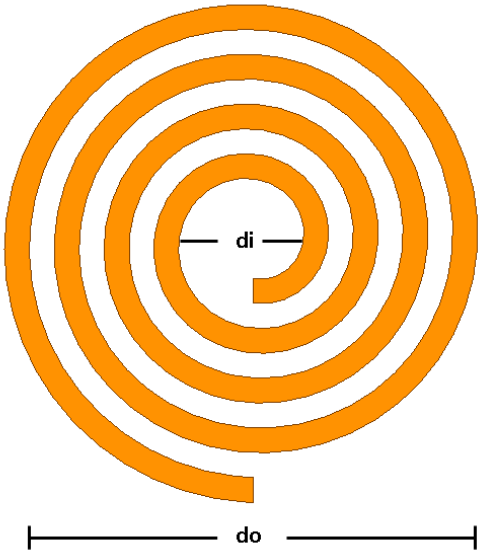

Figure 9: Non-uniform Planar Coil.

The series resistance of the uniform open-type planar coil can be calculated by equation (13) where l_0 is the spiral length which can be calculated using equation (14), ρ_{copper} is the copper resistivity, δ is the skin depth at operating frequency, t is coil thickness, D_k is the loss tangent of the dielectric, and C_s is the equivalent series capacitance of the coil, as shown below:

$$R_s = \frac{\rho_{copper} l_0}{w} \left(\frac{2}{\delta(1 - e^{-\frac{t}{\delta}})} - \frac{4}{3t} \right) + \frac{D_k}{2\pi f C_s} \tag{13}$$

$$l_0 = \frac{\pi n(d_o + d_i)}{2}. \tag{14}$$

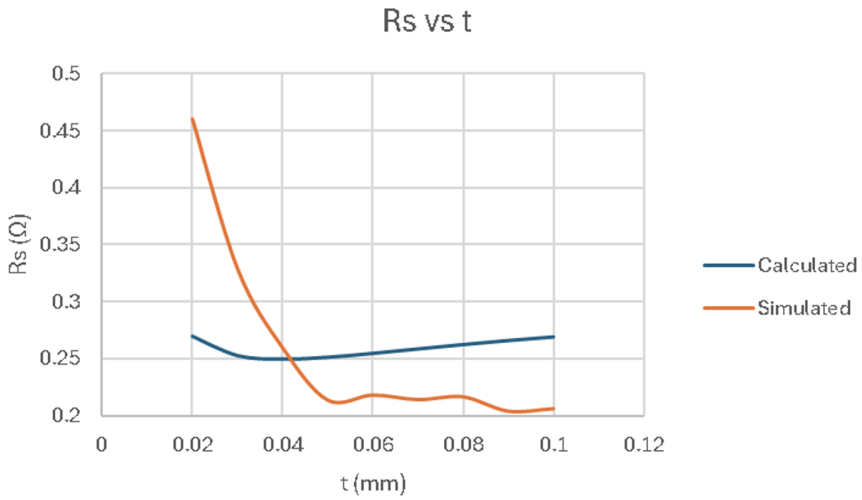

Figure 10: Simulated and Calculated R_s

Using equation (13), the resistance of the coil is calculated for $w_1 = w_2 = 10$ mm, $d_o = 255$ mm, $d_i = 0$ mm, and the number of turns n = 4. The thickness of the coil is swept from 0.01 to 0.1 mm. The calculation and simulation results are compared, as shown in Figure 10. The plot reveals that the calculated value of R_s follows a different trend than the simulation's. In the calculation, the value of R_s tends to increase as the thickness, t, increases, while the simulation shows the opposite trend. In the next chapter, an alternative formula will be derived to better approximate the R_s of the coil.

1.4 Challenges and Opportunities

The rapid adoption of electric vehicles (EVs) has opened new opportunities for wireless power transfer (WPT) technology applications. This alternative charging method offers a more convenient way to charge EVs without the need to move bulky charging cables. However, achieving the same performance in terms of power level and efficiency with WPT systems is not an easy task. The losses and the size of the WPT system on both the TX and receiver RX sides should be low enough so as not to add significant weight or take up too much space in the vehicle. Moreover, high efficiency is desired to minimize energy losses and prevent overheating, which could be harmful to both humans and the vehicle. In addition, the energy transmission distance at which the WPT system can work effectively and efficiently should be sufficient to make the installation of the WPT system easier.

Fortunately, several methods can be used to achieve an effective, efficient, and reliable WPT system. As discussed in the previous chapter, a resonant converter is a good option since it can generate a sinusoidal waveform at ultra-high frequencies, which is beneficial for reducing the size of the components. In addition, this converter can also be tuned to work at zero voltage switching (ZVS) to minimize the switching losses, which are significant at ultra-high frequencies. A Class Φ_2 inverter is chosen from among other resonant converters because it can deliver high power using only one switch at lower voltage levels, thus making it more reliable.

Also, the advantages of non-uniform planar coils have been investigated by [3]. This type of coil can achieve a very high-quality factor, which is crucial for increasing the efficiency and transmission distance of the WPT system. Optimizing this coil's physical design can further increase its quality factor, but this requires good mathematical modeling. In the next few chapters, a new approach to modeling the coil will be investigated. Simulations and experiments will be conducted to verify the mathematical model and optimization.

Chapter 2. Modeling of Ultra High-Frequency Non-uniform Planar Coil

2.1 Mathematical Analysis of Non-Uniform Planar Coils

In the previous chapter, we discussed previous studies that could approximate the inductance and series resistance of non-uniform planar coil with good accuracy. However, the equation could be further improved, as shown in Figure 10, to give us a better approximation. A planar non-uniform coil can be modeled mathematically using the polar coordinates of two individual spirals (inner and outer). The radius of the inner spirals with a number of turns N at any θ can be defined using equations (15) and (16) with some initial radius value of r_0 and constant C which can be rewritten as:

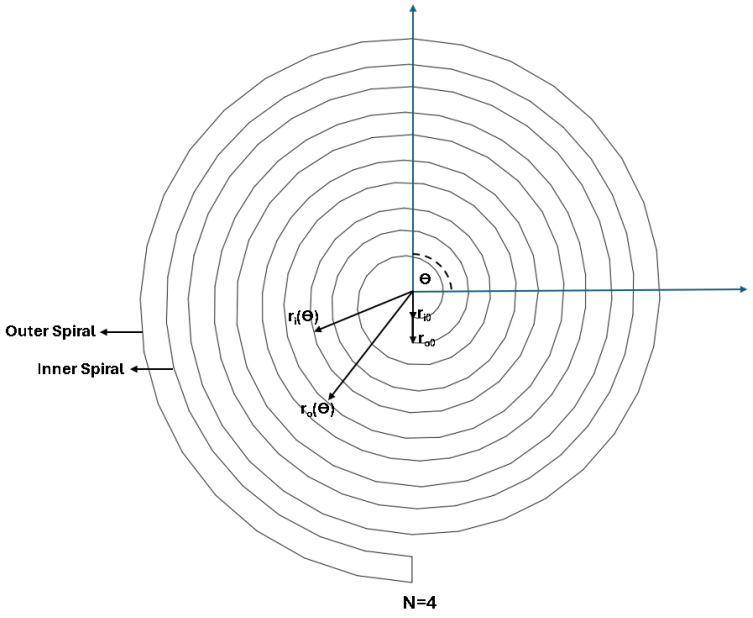

Figure 11: Non-uniform planar coil modeled as two spirals.

$$r_i(\theta) = (r_{i0} + C_i * \theta) \tag{15}$$

$$r_o(\theta) = (r_{o0} + C_o * \theta). \tag{16}$$

Where :

$$\begin{aligned} r_i(\theta) &= \text{Inner spiral radius at } \theta \\ r_{i0} &= \text{Inner coil radius at } \theta = 0 \\ C_i &= \text{Constant of inner spiral} \\ r_o(\theta) &= \text{Outer spiral radius at } \theta \\ r_{o0} &= \text{Outer coil radius at } \theta = 0 \\ C_o &= \text{Constant of outer spiral} \\ \theta &= \text{Angular coordinate from 0 to } 2N\pi \\ N &= \text{Number of turns} \end{aligned} \tag{17}$$

The length of the non-uniform spiral coil can be estimated by taking the mid trace of the inner and outer spiral. First, the initial radius r_{0tr} is calculated by taking the average of the inner and outer spiral initial radius:

$$r_{0tr} = \frac{(r_{o0} + r_{i0})}{2}. \tag{18}$$

Then, the mid-trace constant is calculated using the equation (19):

$$C_{tr} = \frac{((\frac{r_o(2N\pi)+r_i(2N\pi)}{2}) - r_{0avg})}{2N\pi} \tag{19}$$

After obtaining those two values, we can construct the mathematical equation for the mid-trace spiral, as shown below:

$$r_{tr(\theta)} = (r_{tr0} + C_{tr} * \theta). \tag{20}$$

Where:

$$r_t r(\theta) = \text{Trace spiral radius at } \theta$$

$$r_{tr0} = \text{Trace coil radius at } \theta = 0$$

$$C_{tr} = \text{Constant of the trace spiral}$$

Finally, we calculate the length of the mid-trace spiral by using the formula for the arc length of a curve in polar coordinates, which is depicted as:

$$l_0 = \int_0^{2N\pi} \sqrt{(r_{tr0} + C_{tr} * \theta))^2 + C_{tr}^2}\, d\theta. \tag{21}$$

Another important parameter that needs to be calculated from a non-uniform planar coil is its length. A non-uniform planar coil has a non-uniform width; thus, the effective width must be calculated. The width of the non-uniform planar coil at any θ can be calculated by subtracting the outer spiral radius $r_o(\theta)$ from the inner spiral radius $r_i(\theta)$. The effective width of the coil can be approximated as the average coil width along its length, which is given by:

$$w_{eff} = \frac{1}{2N\pi} \int_0^{2N\pi} (r_{o0} - r_{i0}) + (C_o - C_i)\theta)\, d\theta. \tag{22}$$

The physical parameter of the coil using mathematical equations has been derived, such as coil length l_0 and effective width w_{eff}. The next chapter will use those values to calculate the coil inductance and series resistance more accurately.

2.2 Modelling of Inductance and Series Resistance

Even though the inductance of the non-uniform coil has been derived by [7], the value is inaccurate to estimate the true inductance value. To derive an accurate inductance value of the non-uniform coil, this chapter will explain a new formula to calculate the inductance of a non-uniform planar coil by incorporating the mathematical equation explained in Chapter 2.1 for better approximation. Furthermore, this chapter will also explain the derivation of the equation to precisely estimate the series resistance of the coil. This new formula will provide a more accurate equation for determining the inductance and series resistance of non-uniform planar coils, which is crucial for optimizing the performance of high-frequency wireless power transfer systems.

The inductance formula for a non-uniform planar coil is given by [3] as can be seen in equation (12). To maintain consistency and to reflect the spiral equations that govern the coil, equation (12) can be rewritten as:

$$L = \frac{N^2 A(ln(\frac{2.46A}{B}) + 0.2(\frac{B}{A})^2)}{4} \tag{23}$$

where equation (24) and (25) are the equivalent forms of d_i-d_o and d_i+d_o respectively as shown below:

$$A = (2(r_{i0} + r_{o0}) + \pi(C_i + (4N - 1)C_o) \tag{24}$$

$$B = 2(r_{o0} - r_{i0}) + \pi((4N - 1)C_o - C_i). \tag{25}$$

The DC resistance of a simple planar coil can be calculated using the equation (26). The losses of open-coil copper are different from single planar coil since the current along the path is not uniform:

$$R = \frac{\rho l_0}{w_{eff} t}. \tag{26}$$

Assuming linear decrease [7] in an upper coil that is connected to the source, the current at the top and bottom coil can be approximated as:

$$I_{top} = \frac{l}{l_0} I \tag{27}$$

$$I_{bot} = \frac{l - l_0}{l_0} I. \tag{28}$$

The losses at the open-type planar non-uniform coil then can be calculated using equation (29) where l_{0top} is the upper coil length, l_{0bot} is the lower coil length, w_{efftop} is the upper coil effective width, and w_{effbot} is the lower coil effective width. The losses of the open-type coil are calculated by integrating the squared current of each coil along its length and then multiplying it with $\frac{\rho}{w_{eff}t}$ which gives us the losses as below:

$$P = \frac{\rho}{w_{efftop}t} \int_0^{l_{0top}} (I_{top})^2 \, dl + \frac{\rho}{w_{effbot}t} \int_0^{l_{0bot}} (I_{bot})^2 \, dl \tag{29}$$

$$P = I^2 \rho (\frac{l_{0top}}{3w_{efftop}t} + \frac{l_{0botI^2}}{3w_{effbot}t}). \tag{30}$$

As shown in the equations, the total DC resistance of the coil is one-third of the DC resistance of the top coil plus one-third of the DC resistance of the bottom coil, as given below:

$$R = \rho (\frac{l_{0top}}{3w_{efftop}t} + \frac{l_{0bot}}{3w_{effbot}t}). \tag{31}$$

The effect of skin depth due to eddy current will affect the effective thickness. This effective thickness can be calculated using equation (32) as studied by [11]. Furthermore, the resistance of the open-type coil due to the skin effect can be approximated as two times of a single coil [7], where the skin depth is:

$$t_{eff} = \frac{1}{\delta(1 - e^{\frac{-t}{\delta}})}. \tag{32}$$

Thus the total series resistance of the open coil can be calculated as:

$$R_s = 2\rho\left(\frac{l_{0top}}{3w_{efftop}t_{eff}} + \frac{l_{0bot}}{3w_{effbot}t_{eff}}\right). \tag{33}$$

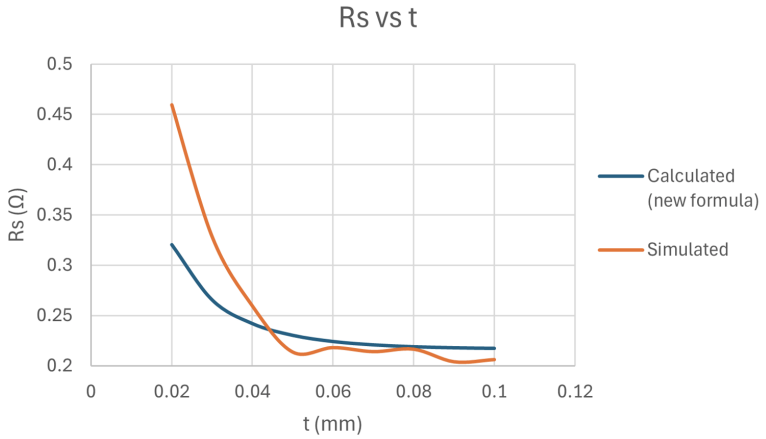

Figure 12: Simulated and Calculated R_s Using New Equation (N = 4, dist = 1 mm).

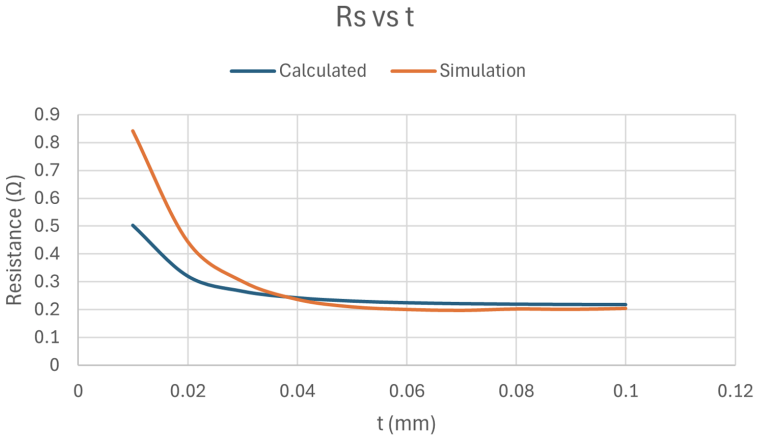

Figure 13: Simulated and Calculated R_s Using New Equation (N = 4, dist = 1.5 mm).

The resistance of the coil with the same parameters as in Chapter 1 is calculated using the new equation. Figures 12 and 13 show that there is a good agreement between the calculated and simulated value even when the distance between the coil is increased, which confirms the accuracy of the new mathematical model of the coil.

Chapter 3. Optimization of Non-uniform Planar Coil Quality Factor

3.1 Defining the Optimization Problem for the Quality Factor

The equations to calculate the inductance and series resistance of a non-uniform planar coil have been derived in Chapter 2. These equations can approximate the inductance and series resistance values with good accuracy. The quality factor of a coil can be defined as the ratio between the coil's impedance and its resistance at the operating frequency ($Q = \frac{X_L}{R_s}$). To achieve a high-quality factor, a coil must have a high inductance value with minimal series resistance. Thus, the optimization of the coil quality factor can be formulated as a maximization problem. The goal is to maximize a quality factor within the constraints described below.

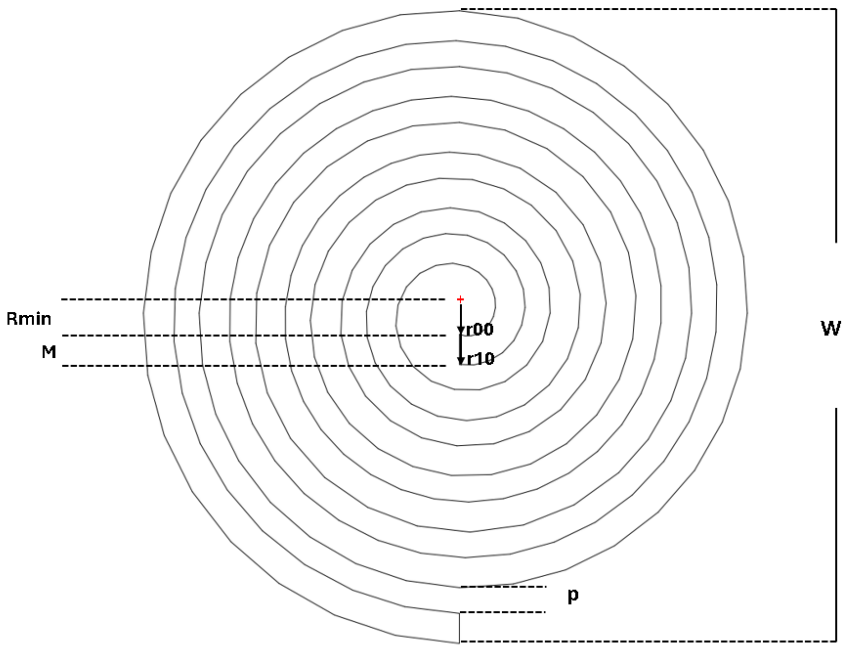

Figure 14: Coil Parameters.

Constraints: (1) C1, C2, C3, and C4 are the coefficients that define how much

the radius increases as the theta increases. The values of C_0, C_1, C_2, C_3, and t must be positive to ensure that the coil design is physically feasible (equation 35).

(2) The values of r_{00}, r_{10}, r_{20}, r_{30} must be bigger than R_{min} to set the minimum inner radius of the coil (equation 36).

(3,4) The values of r_{10} and r_{30} must be bigger than r_{00} and r_{20} respectively to construct the inner and outer spiral of the coils (equation 37 and 38).

(5) To make sure that the radius of the spirals increases at the same rate, the values of C_0, C_1, C_2, and C_3 are set to be equal (equation 39).

(6) The non-uniform width of the coil is achieved by setting the width of the top coil larger than the width of the bottom coil(equation 40).

(7) The pitch (p) of the coil must be the same as the width of the coil (equation 41).

(8) Due to the limitation of the copper sheet, the copper outer diameter cannot be larger than the width of the copper sheet(equations (42)).

(9) The width of the coil is set to be larger or equal to some value to accommodate manufacturing constraints, as some machines are unable to cut very narrow dimensions (equation 43).

(10) Finally, constraint 10 governs the number of turns for the coil (equation 44).

The maximization problem and its constraints are depicted below:

$$\text{Maximize } Q(L, R_s) = \frac{2\pi f L}{R_s} \tag{34}$$

Subject to:

$$C_0, C_1, C_2, C_3, t > 0 \tag{35}$$

$$r_{00}, r_{10}, r_{20}, r_{00} > R_{min} \tag{36}$$

$$r_{10} > r_{00} \tag{37}$$

$$r_{30} > r_{20} \tag{38}$$

$$C_0 = C_1 = C_2 = C_3 \tag{39}$$

$$r_{30} - r_{20} > r_{10} - r_{00} \tag{40}$$

$$(r_{10} - r_{00}) - \pi((2N-1)C_1 - 2NC_0) = 0 \tag{41}$$

$$2r_{10} + C_1\pi(4N-1) \leq W \tag{42}$$

$$r_{10} - r_{00} \geq M \tag{43}$$

$$N = 2, 3, 4, \ldots \tag{44}$$

Where:

C_0, C_2 = Constant of the inner spiral of bottom and top coil, respectively

C_1, C_3 = Constant of the inner spiral of bottom and top coil, respectively

r_{00}, r_{20} = Radius of the inner spiral of bottom and top coil, respectively, at $\theta = 0$

r_{10}, r_{30} = Radius of the outer spiral of bottom and top coil, respectively, at $\theta = 0$

θ = Angular coordinate from 0 to $2n\pi$

N = Number of turns

L = Inductance

R_s = Series resistance

t = Copper thickness

D = Width of copper sheet

R_{min} = Minimum radius of the spiral

M = Coil minimum width.

3.2 Maximizing the Value of the Quality Factor

The optimization problem of the coil involves many complex equations, especially the equation (21) to calculate the trace length. Since it is challenging to solve the equation mathematically by hand, Python programming language is preferred to be used. This language offers various optimization libraries and tools that can be chosen for solving the equation. Among them are CVXPY and SciPy. CVXPY is a popular library that is used to solve optimization problems with convex equations. This library is easy to use since it uses syntax that is close to mathematical notation. To use this library, all the equations that are related to the optimizations must be written to follow discipline convex programming (DCP) rules to make sure that the library understands the problem.

SciPy is another popular library that can be utilized to solve an optimization problem. This library can solve various optimization including non-convex equations. However, this library requires more effort to manually set up the optimization problems. The first attempt is made to use the CVXPY optimization, unfortunately, the L/R_s is a nonconvex equation thus the optimization can not be solved using this library. The SciPy library is then used to solve the optimization problem. Some of the constraints in the equation (34) are simplified due to manufacturing and material availability. For example, the thickness of the copper is set to be 0.5 mm since copper sheets with that thickness are common and easy to purchase. The maximum outer diameter of the coil is set to 250 mm due to the copper size limit. The minimum width of the coil is 10 mm, respectively, due to machine limitations.

Using this information, an optimization program using the SciPy library is conducted. The results in Figures 15, 16, and 17 are then obtained. From those three figures, we can see that the inductance and resistance of the coils increase as the number of turns increases. However, we can see that the value of the quality factor starts to decrease from N=5 t0 N=6; thus, increasing N larger than 5 will not give a higher quality factor. The maximum quality factor of the coil is achieved at $r_{00} = r_{20} = 15$ mm, $r_{10} = 25$ mm, $r_{30} = 27$ mm, $C_0 = C_1$, C_2, $C_3 = 3.18$ mm.

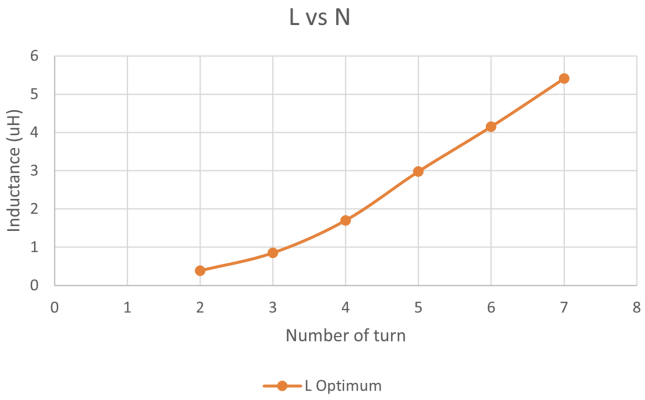

Figure 15: Optimum L value.

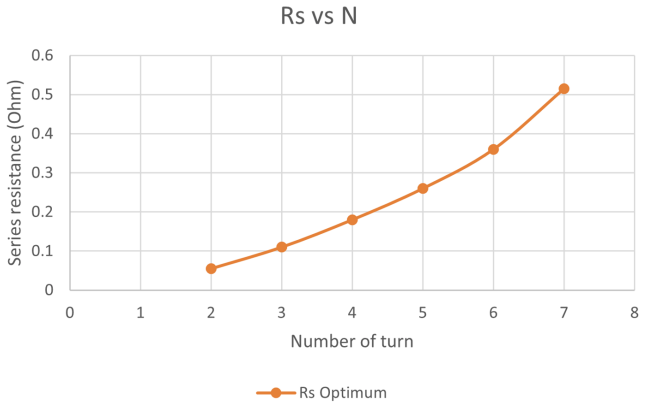

Figure 16: Optimum R_s value.

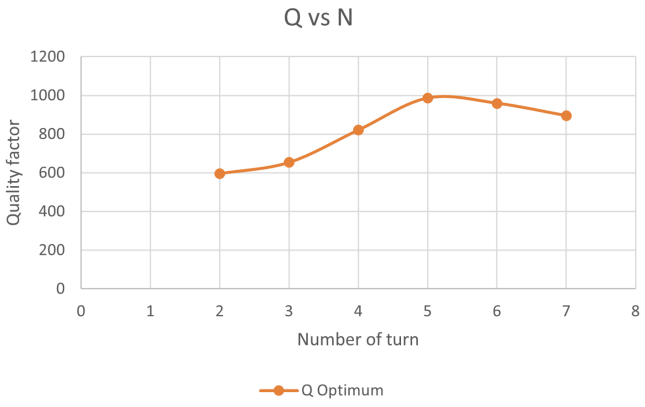

Figure 17: Optimum Q value.

Chapter 4. Results

In previous chapters, we demonstrate the advantages of class Φ_2 as an inverter for the WPT system. Not only is it more reliable since it uses fewer switches, but it also has lower voltage stress across the device, which makes it suitable for high-power applications. Also the non-uniform planar coil also offers a high-quality factor, which is beneficial for maximizing the WPT system efficiency. This chapter will discuss simulations that have been conducted to verify the performance of the class Φ_2 inverter. The quality factor of the coils is also investigated by running simulations using Ansys HFSS. Lastly, the experiment to validate the operation of the WPT systems will also be explained.

4.1 Class Φ_2 Inverter Design

The inverter is designed to provide 1 kW output power, which is considered the rated power of the inverter and is suitable for a level 1 EV charger. The input voltage of the class Φ_2 inverter is designed to be 250 V, and a 20 Ω R_L is chosen. Additionally, 13.56 MHz frequency is chosen since it aligns with the international, scientific, and medical (ISM) bands, thus making the development easier from a regulatory point of view.

The operation of a high-power resonant converter at MHz frequency is sometimes limited by switching device availability. The switch must have a low output capacitance C_{oss} so that it can turn on and off quickly at 13.56 MHz. As what has been investigated by [4], an enhancement mode Gallium Nitrite Field Effect Transistor (eGaN FET) GS66508T is selected due to its low output capacitance (C_{oss}), on-resistance (R_{dson}), and inductance. The rated voltage of GS66508T is 650 V, thus a 250 V input voltage is suitable since the V_{ds} peak voltage at class Φ_2 is still lower (500 V) than the rated voltage.

Based on those design criteria, the size of the class Φ_2 inverter's components

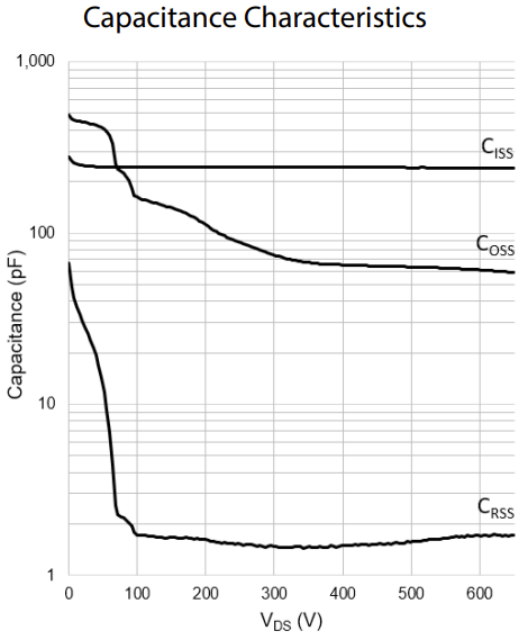

Figure 18: GS66508T Output Capacitance. [14]

is then calculated using the equation (3) to (4). The value of the switch's C_{oss} is considered when during the tuning process, which yields the values in table 2. We can also notice that the size of the components, especially the inductors, is small, thus making the size of the inverter still relatively small even though it uses more passive components compared to class E inverter.

Table 2. Component Selection

Parameter	**Value**	**Type**
V_i	250 V	NA
P_{out}	1 kW	NA
L_S	290 nH	Custom inductor with air core
L_F	240 nH	Custom inductor with air core
L_{MR}	200 nH	Custom inductor with air core
C_P	332 pF	1812GA151JAT1A 220 pF + 1812HA220JAT1A 47 pF + 65 pF Coss of GS66508T
C_{MR}	172 pF	1812HA221JAT1A 220 pF + 1812HA220JAT1A 22 pF
C_S	10 nF	C1812X103JCGAC7800 10 nF
R_L	20 Ω	2x50 and 100 Ω RF load in parallel
Q	eGAN FET	GS66508T

4.2 Simulation Verification

LTspice is used to verify the performance of the class Φ_2 inverter from Chapter 4.1. The value of R_l is varied to investigate the output power and efficiency of the converter under various load resistances. Figure 19 shows that a relatively high output power and efficiency can be maintained under big load resistance variance. It is also observed that the inverter operates in ZVS, as shown in Figure 20.

The optimum design of the coil has been obtained in the previous chapter. The N value of 5 is selected since it gives the highest quality factor. This optimization result is then verified by simulation using ANSYS HFSS. The coil is modeled using a mathematical equation using all the parameters obtained in Chapter 3.

Figures 21 to 23 show that the simulation results closely match the optimization. The only difference is at simulation, the quality factor starts to drop after N=6; meanwhile, at optimization, it is N=5. The difference could be attributed to the L value, which is shown by Figure 21. At optimization, the L value increases slower

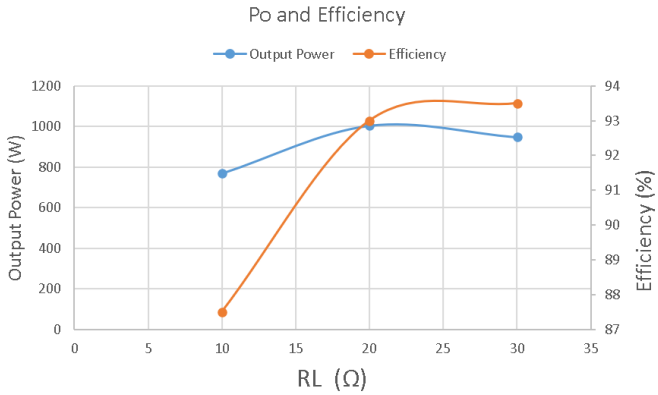

Figure 19: Simulated Output Power and Efficiency of Class Φ_2 Inverter.

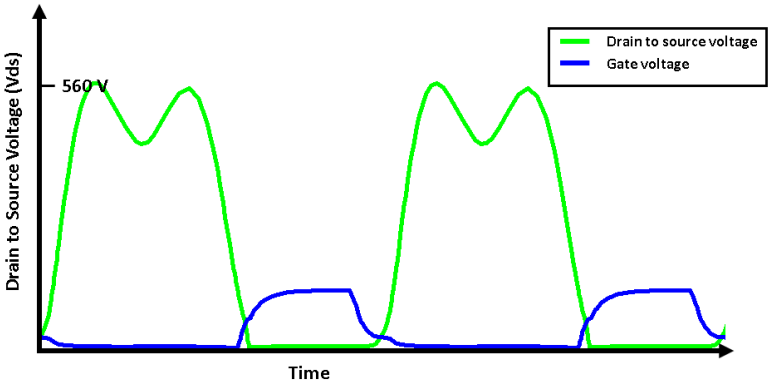

Figure 20: V_{DS} and V_g of the Class Φ_2 Inverter.

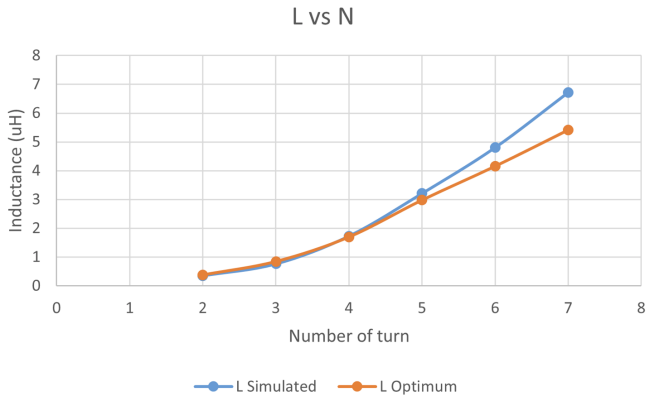

Figure 21: Simulated L value.

at N bigger than 5, thus affecting the quality factor. Initially, a coil with a number of turns N=5 is selected since it gives a value closer to the simulation; however, a

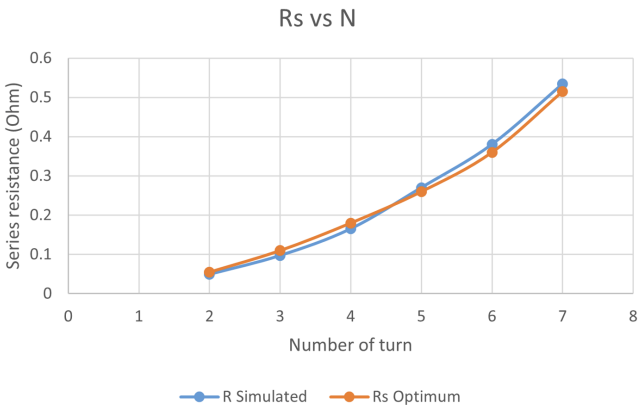

Figure 22: Simulated R_s value.

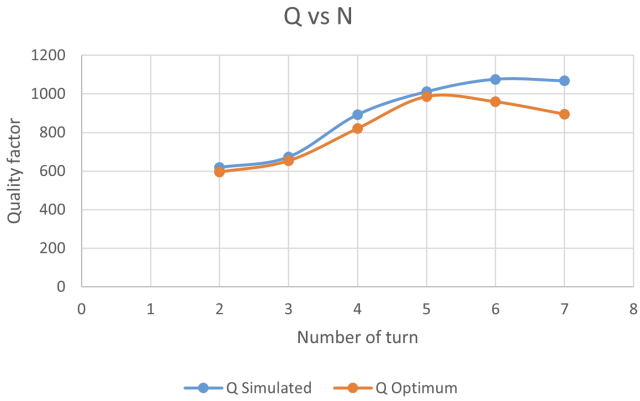

Figure 23: Simulated Q value.

large gap (9.5 mm) between the top and bottom coils is required to make the coil resonate at 13.56 MHz. The next option goes to N=4, at this number of turns the gap that is needed is only 2.5 mm which makes the coil construction easier. The parameters of coil with N=4 are $r_{00} = r_{20} = 15$ mm, $r_{10} = 25$ mm, $r_{30} = 27$ mm, $C_0 = C_1$, C_2, $C_3 = 3.18$ mm

4.3 Experimental Validation

The complete parts of WPT systems have been investigated in the previous chapters. We discovered that mathematical and simulation methods share a good agreement for designing the class Φ_2 inverter and non-uniform planar coil. This chapter will talk about several experiments that have been conducted to validate the calculation and simulations. A class Φ_2 inverter was built using the components with sizes in Table 2. First, the inverter was connected directly to the radio frequency (RF) load without the coil. The inverter was operated in burst mode with 1000 pulses from a keysight 81160A signal generator. The input voltage of 230 V from a keysight N5771A power supply was applied to the inverter. The voltage and current at the input and output sides of the inverter were then measured using the Keysight MSOX3034T oscilloscope. The input power is calculated by multiplying the input voltage with the input current. The output power is calculated by dividing the square of the RMS output voltage by the load resistance. With this setup, an output power of 935 W with an efficiency of 93.7 % was achieved. The output voltage V_o, input current I_i, drain to source voltage V_{ds}, and gate to source voltage V_{gs} are shown in Figure 25. As shown in the figure, the inverter can operate at ZVS, which improves efficiency.

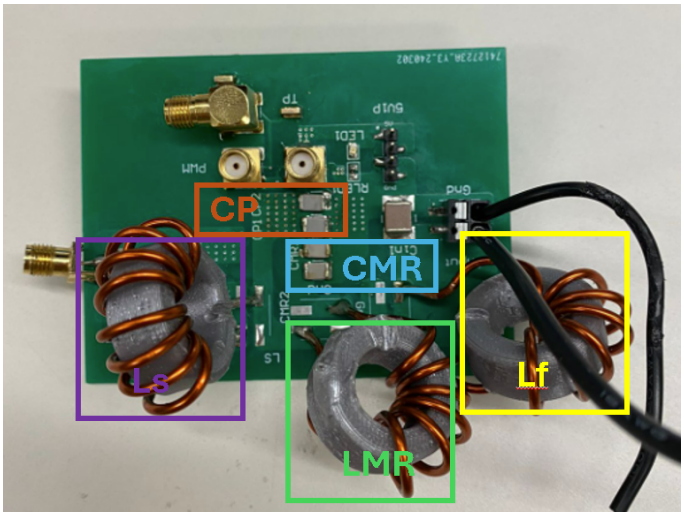

Figure 24: Top view of the class Φ_2 PCB.

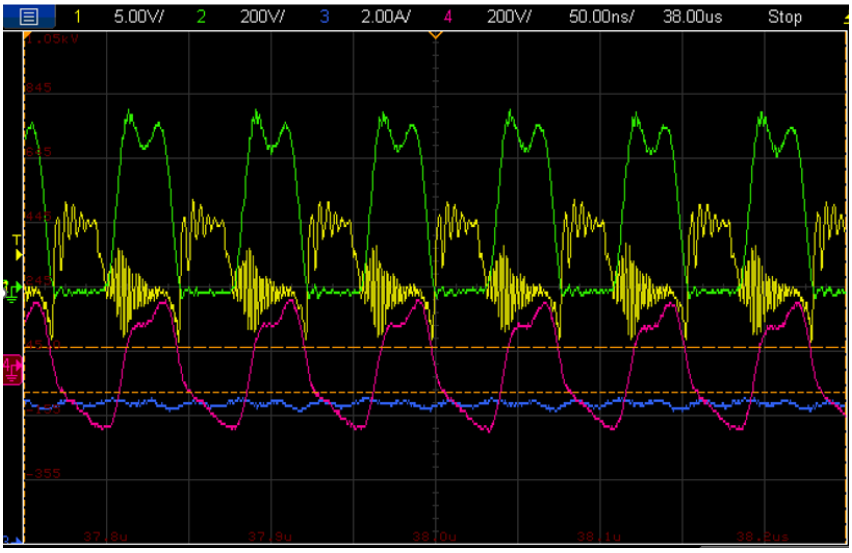

Figure 25: Inverter: V_o (pink), I_i (blue), V_{ds} (green), and V_{gs} (yellow).

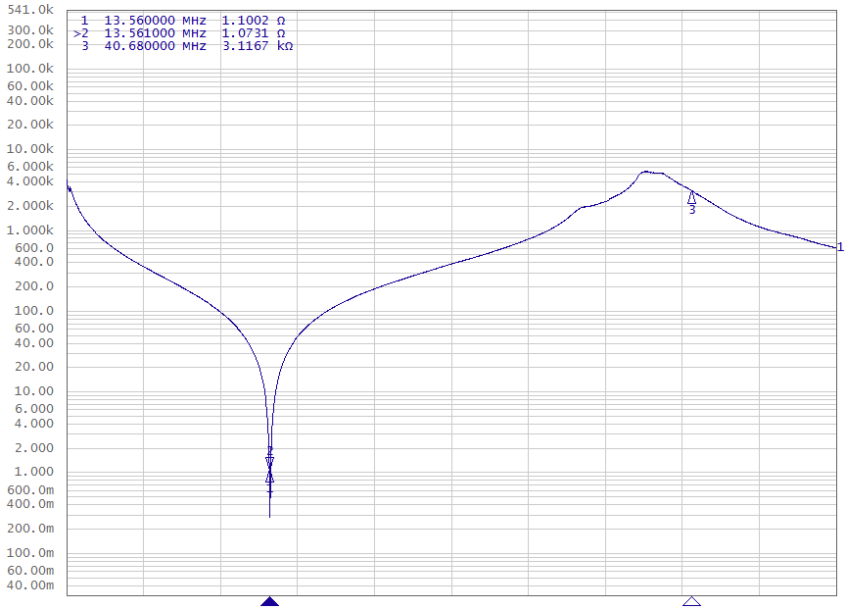

Figure 26: Coil Impedance.

After that, we fabricated the Tx and Rx coil from a 300 x 300 x 0.5 mm copper sheet using an OMAX ProtoMAX water jet cutter. The rough edges were cleaned using p400 sandpaper, and a finishing touch was applied using p3000 sandpaper to polish the surface of the coils. The coils were then affixed to acrylic sheets to secure them firmly. The resonant frequency of 13.56 MHz was achieved when the top and bottom coils were separated by a 2.47 mm air gap as depicted in Figure 26. A virtual network analyzer was used to measure the coil's inductance and series resistance.

First, we measured the coil connector to investigate the additional inductance and series resistance introduced by the connector. After that, we measure the inductance and series resistance of the coil with the connector. The parameters of the coil are the difference between the coil and connector with the connector. From Table 3, the coils' inductance, series resistance, and quality factor match the calculation and simulation closely. A high-quality factor (776 & 925) is achieved using copper sheets. However, the Q value is significantly reduced when the connector is used due to additional series resistance.

Table 3. Coil Parameters.

Parameter	**Connector**	**Coil + Connector**	**Coil**
L	0.391 μH	**Tx** (2.121 μH), **Rx** (2.153 μH)	**Tx** (1.73 μH), **Rx** (1.76 μH)
R_s	253 mΩ	**Tx** (443 mΩ), **Rx** (415 mΩ)	**Tx** (190 mΩ), **Rx** (162 mΩ)
Q	NA	**Tx**(408), **Rx** (442)	**Tx**(776), **Rx** (925)

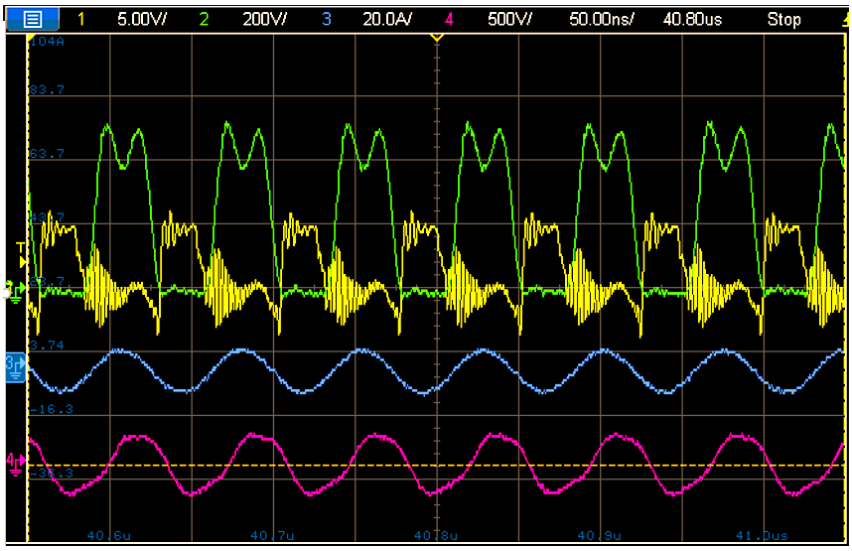

Figure 27: Inverter with Resonant Coupling Coils: V_o (pink), I_o (blue), V_{ds} (green), and V_{gs} (yellow).

Finally, we tested the complete setup of the WPT system using the inverter and coils. The Rx coil is connected to a 50 Ω RF load; thus, a matching network is used such that the output of the inverter will see a 20 Ω load. The distance between the Tx and Rx coil is set to be 63 mm. The experimental setup can be seen in Figure

28. The output voltage is calculated by multiplying the squared output current (I_o) with load resistance (R_L). An output power of 1072 W was measured when we applied a 230 V input voltage to the inverter. with this setup, we achieve 96% coil efficiency, which proves the effectiveness of the coil. In Figure 27, we can also see that the inverter was able to maintain ZVS condition; the drain to source voltage of the inverter was also below the rated voltage (560 V).

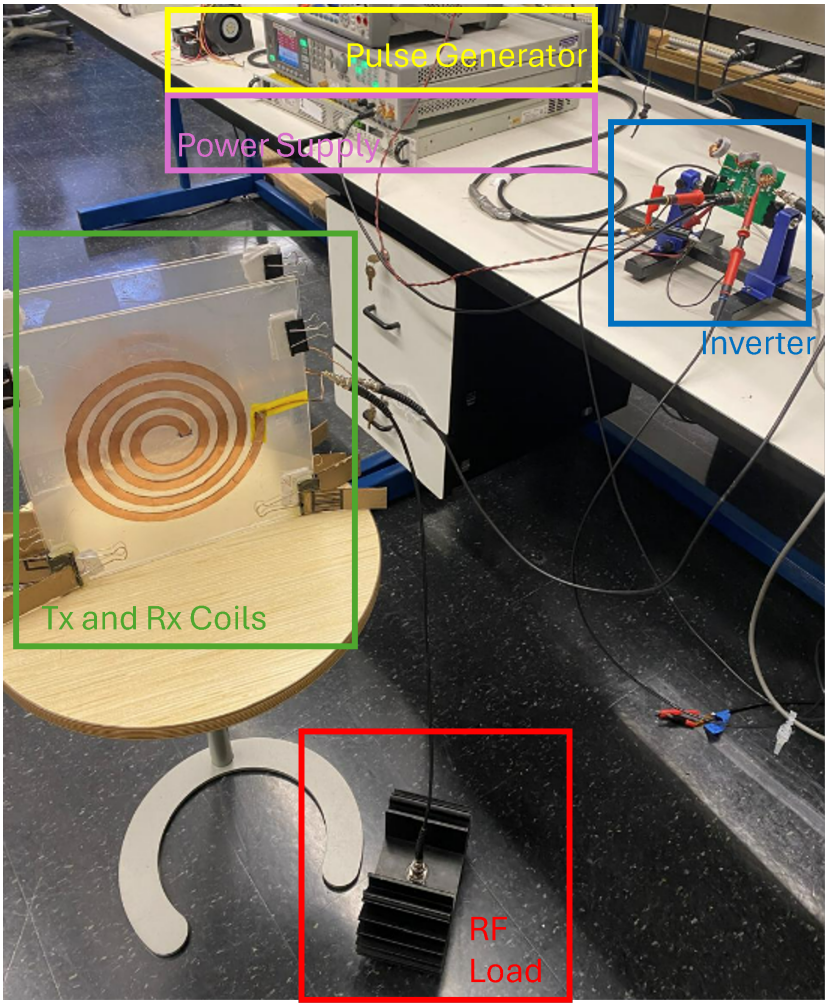

Figure 28: Experimental Setup.

Chapter 5 Discussion and Conclusion

A step-by-step approach to designing a WPT system has been explained. Moreover, a new equation to accurately model the coil has been derived. The optimum design for the non-uniform planar coil was obtained using mathematical optimization and verified by simulation. The experimental validation shows that the coil quality factor matches the calculation and simulation closely. However, the quality factor is greatly reduced when using a connector. In future work, improving the connector to minimize the additional inductance and series resistance will be investigated to increase the overall quality factor of the coil. Additionally, the optimization will include the capacitance of the coil to better predict the resonant frequency and the gap required between the top and bottom coils.

Finally, the complete setup of the WPT system has been realized using a class Φ_2 inverter with a non-uniform planar coil. The system is designed to operate at 13.56 MHz with an output power of 1000 W. The complete setup was able to deliver 1072 W of output power with 96% efficiency over a 63 mm distance when a 230 V input voltage was applied to the inverter. For future work, we plan to increase the inductance of the coil while maintaining a high-quality factor so that the transmission distance can be increased.

References

[1] Center for Sustainable Systems, University of Michigan. 2023. “Carbon Footprint Factsheet.” Pub. No. CSS09-05.

[2] The World Bank. 2021. “https://wdr2021.worldbank.org/World Development Report 2021 .” https://wdr2021.worldbank.org/spotlights/datas-carbon-footprint/.(accessed July. 30, 2024).

[3] R. Qin, J. Li and D. Costinett, ”A 6.6-kW High-Frequency Wireless Power Transfer System for Electric Vehicle Charging Using Multilayer Nonuniform Self-Resonant Coil at MHz,” *IEEE Transactions on Power Electronics*, vol. 37, no. 4, pp. 4842-4856, April 2022, doi: 10.1109/TPEL.2021.3120734.

[4] J. Choi, D. Tsukiyama, Y. Tsuruda and J. M. R. Davila, ”High-Frequency, High-Power Resonant Inverter With eGaN FET for Wireless Power Transfer,” *IEEE Transactions on Power Electronics*, vol. 33, no. 3, pp. 1890-1896, March 2018, doi: 10.1109/TPEL.2017.2740293.

[5] I. Sasahara and K. Akatsu, ”A Coupler design for high power 2.3 kW WPT using 13.56 MHz,” *2022 IEEE 31st International Symposium on Industrial Electronics (ISIE)*, Anchorage, AK, USA, 2022, pp. 762-767, doi: 10.1109/ISIE51582.2022.9831577.

[6] J. M. Rivas, Y. Han, O. Leitermann, A. D. Sagneri and D. J. Perreault, ”A High-Frequency Resonant Inverter Topology With Low-Voltage Stress,” *IEEE Transactions on Power Electronics*, vol. 23, no. 4, pp. 1759-1771, July 2008, doi: 10.1109/TPEL.2008.924616.

[7] J. Li and D. Costinett, ”Analysis and design of a series self-resonant coil for wireless power transfer,” in *2018 IEEE Applied Power Electronics Conference and Exposition (APEC)*, San Antonio, TX, USA, 2018, pp. 1052-1059, doi: 10.1109/APEC.2018.8341145.

[8] C. R. Sullivan, B. A. Reese, A. L. F. Stein and P. A. Kyaw, "On size and magnetics: Why small efficient power inductors are rare," in *2016 International Symposium on 3D Power Electronics Integration and Manufacturing (3D-PEIM)*, Raleigh, NC, USA, 2016, pp. 1-23, doi: 10.1109/3DPEIM.2016.7570571.

[9] R. Qin and D. Costinett, "Multi-layer Non-uniform Series Self-resonant Coil for Wireless Power Transfer," in *2019 IEEE Energy Conversion Congress and Exposition (ECCE)*, Baltimore, MD, USA, 2019, pp. 3333-3339, doi: 10.1109/ECCE.2019.8913274.

[10] N. Sokal and A. Sokal, "Class E—A new class of high-efficiency tuned single-ended switching power amplifiers," *IEEE J. Solid-State Circuits*, vol. 10, no. 3, pp. 168–176, Jun. 1975.

[11] C. P. Yue and S. S. Wong, "Physical modeling of spiral inductors on silicon," *IEEE Transactions on Electron Devices*, vol. 47, no. 3, pp. 560–568, 2000.

[12] ZEV Alliance, "Understanding the Business Case for Electric Vehicle Charging Infrastructure," www.zevalliance.org.https://zevalliance.org/wp-content/uploads/2024/01/Understanding-the-Business-Case-for-Electric-Vehicle-Charging-Infrastructure

[13] S. Mukherjee, A. Kumar, and S. Chakraborty, "Comparison of DAB and LLC dc-dc converters in high-step down fixed-conversion-ratio (DCX) applications," *IEEE Trans. Power Electron.*, vol. 36, no. 4, pp. 4383–4398, Apr. 2021.

[14] GaN Systems, "GS66508T Top-side cooled 650 V E-mode GaN transistor Datasheet," Rev 200402. https://gansystems.com/gan-transistors/gs66508t/ (accessed June. 7, 2024).

[15] T. Kondo and H. Koizumi, "Class DE voltage-source parallel resonant inverter," IECON 2015 - 41st Annual Conference of the IEEE Industrial Electronics Society, Yokohama, Japan, 2015, pp. 002968-002973, doi: 10.1109/IECON.2015.7392554.

[16] M. Kim and J. Choi, "High-Frequency, Mid-range Wireless Power Transfer System using Critical Coupling Coefficient Adjustment," 2021 IEEE Applied Power Electronics Conference and Exposition (APEC), Phoenix, AZ, USA, 2021, pp. 714-719, doi: 10.1109/APEC42165.2021.9487028.